



HAL
open science

Star Formation and Dust Attenuation Properties in Galaxies from a Statistical UV-to-FIR Analysis

Denis Burgarella, Veronique Buat, Jorge Iglesias-Paramo

► **To cite this version:**

Denis Burgarella, Veronique Buat, Jorge Iglesias-Paramo. Star Formation and Dust Attenuation Properties in Galaxies from a Statistical UV-to-FIR Analysis. *Monthly Notices of the Royal Astronomical Society*, 2005, 360, pp.1413. 10.1111/j.1365-2966.2005.09131.x . hal-00015259

HAL Id: hal-00015259

<https://hal.science/hal-00015259>

Submitted on 13 Dec 2020

HAL is a multi-disciplinary open access archive for the deposit and dissemination of scientific research documents, whether they are published or not. The documents may come from teaching and research institutions in France or abroad, or from public or private research centers.

L'archive ouverte pluridisciplinaire **HAL**, est destinée au dépôt et à la diffusion de documents scientifiques de niveau recherche, publiés ou non, émanant des établissements d'enseignement et de recherche français ou étrangers, des laboratoires publics ou privés.

Star formation and dust attenuation properties in galaxies from a statistical ultraviolet-to-far-infrared analysis

D. Burgarella,¹★ V. Buat¹★ and J. Iglesias-Páramo²★

¹*Observatoire Astronomique Marseille Provence, Laboratoire d'Astrophysique de Marseille, 13012 Marseille, France*

²*Instituto de Astrofísica de Adalucía (CSIC), 18008 Granada, Spain*

Accepted 2005 April 15. Received 2005 April 11; in original form 2005 March 4

ABSTRACT

We study two galaxies samples selected in near-ultraviolet (NUV) and in far-infrared (FIR) for which the spectral energy distributions (SEDs) from the far-UV (FUV) to the FIR are available. We compared the observed SEDs to modelled SEDs with several star formation histories (SFHs; decaying star formation rate plus burst) and dust attenuation laws (power law + 2175 Å bump). The Bayesian method allows one to estimate statistically the best parameters by comparing each observed SED to the full set of 82 800 models. We reach the conclusion that the UV dust attenuation cannot be estimated correctly from SED analysis if the FIR information is not used. The dispersion is larger than with the FIR data. The distribution is also not symmetrically distributed about zero: there is an overestimation for UV-selected galaxies and an underestimation for FIR-selected galaxies. The output from the analysis process suggests that UV-selected galaxies have attenuation laws in average similar to the Large Magellanic Cloud extinction law while FIR-selected galaxies attenuation laws resemble more the Milky Way extinction law. The dispersion about the average relation in the log ($F_{\text{dust}}/F_{\text{FUV}}$) versus FUV–NUV diagram (once the main relation with FUV – NUV accounted for) is explained by two other parameters: the slope of the attenuation law and the instantaneous birthrate parameters b_0 for UV-selected galaxies and the same ones plus the strength of the bump for the FIR-selected galaxies. We propose a recipe to estimate the UV dust attenuation for UV galaxies only (that should only be used whenever the FIR information is not available because the resulting A_{FUV} is poorly defined with an uncertainty of about 0.32): $A_{\text{FUV}} = 1.4168 (FUV - NUV)^2 + 0.3298 (NUV - I)^2 + 2.1207 (FUV - NUV) + 2.7465 (NUV - I) + 5.8408$.

Key words: galaxies: starburst – infrared: galaxies – ultraviolet: galaxies.

1 INTRODUCTION

Spectral energy distributions (SEDs) are commonly compared to templates or models to estimate galaxy physical parameters like, for instance, the dust attenuation and the star formation history (SFH). In recent years, this method has been applied to galaxy samples at low redshift [e.g. Kauffmann et al. 2003a on SDSS data and Salim et al. 2005 on the *Galaxy Evolution Explorer* (GALEX) + SDSS data]. But the availability of multiwavelength deep fields (e.g. the *Hubble Deep Field*, Williams et al. 1996) also opened up the possibility of applying this method on galaxy samples at much higher redshifts (e.g. Shapley et al. 2001; Forster Schreiber et al. 2004; Barmby et al. 2001). Still, none of these works use far-infrared (FIR) data that would bring a strong constraint on the absolute amount of

dust attenuation. For instance, Granato et al. (2000) and Efstathiou & Rowan-Robinson (2003) use additional FIR data to better understand physical differences between SEDs.

Ultraviolet (UV) photons are emitted by young stars and the UV flux give information on the evolution of the star formation rate (SFR). However, to make full use of this UV data, we must apply a correction for the dust attenuation that converts UV photons into FIR photons through absorption. Note that this dust attenuation includes the effects of scattering and absorption in an effective absorption. Several methods to correct the UV flux for dust attenuation have been presented. The slope of the UV continuum β (Calzetti, Kinney & Storchi-Bergmann 1994; Meurer, Heckman & Calzetti 1999) or its proxy, the far-ultraviolet – near-ultraviolet (FUV – NUV) colour have been proposed to trace the UV dust attenuation. However, Bell (2002), Goldader et al. (2002), Kong et al. (2004) started to show that this method cannot be generalized to every galaxy types outside starbursts. This was recently confirmed from the GALEX photometric data by Buat et al. (2005), Seibert et al. (2005) and

★E-mail: denis.burgarella@oamp.fr (DB); veronique.buat@oamp.fr (VB); jiglesia@iaa.es (JI-P)

from *GALEX* spectroscopy by Burgarella et al. (2005). Buat & Xu (1996) proposed using the dust-to-UV flux ratio ($F_{\text{dust}}/F_{\text{UV}}$) and this method appears to be more stable and accurate than the latter one (Witt & Gordon 2000; Buat et al. 2005).

By including FIR data into the SED analysis, we start to raise the degeneracy and relieve the pressure on the UV/optical range, which can therefore be used to constrain the shape of the attenuation law and the SFH.

Of course, to apply this method means that FIR data are available for the studied UV galaxy sample which is not always true. Therefore, we could wonder what error is made if we do not use FIR data?

We use a Bayesian method to compare the SEDs (from FUV to FIR) of two purely defined samples selected in UV and in FIR to a set of 82 800 models with several dust attenuation laws, dust attenuations and SFHs. We deduce physical parameters for these two samples of galaxies. The analysis is carried out by accounting for the FIR information and then without the FIR information. We quantitatively estimate errors in the parameters implied by an analysis without FIR and outline where knowledge of the FIR data brings some noticeable differences.

The successful launch of the *GALEX* Martin et al. 2004, will lead to an important increase in the UV data base available to the astronomical community. New galaxy populations are showing up and we can launch a statistically significant study of local galaxies observed in the rest-frame UV: diagrams which were previously scarcely populated with strongly biased samples of galaxies are now much more populated. This knowledge could, in turn, be used to better understand the rest-frame UV Universe up to the highest observed redshift (*Hubble Space Telescope* Ultra Deep Field, Bunker et al. 2004; Bouwens et al. 2004; Yan et al. 2004).

In the first part of this paper, we will show that the error on the UV dust attenuation estimated without the FIR information is significant. Then, we estimate quantitatively the error for two pure galaxy samples selected in near-UV (NUV) from *GALEX* data and in FIR from *IRAS* data. Finally, we determine a relation that allows to evaluate, at best, the UV dust attenuation for UV-selected galaxies when no FIR is available.

We assume a cosmology with $H_0 = 70 \text{ km s}^{-1} \text{ Mpc}^{-1}$, $\Omega_M = 0.3$ and $\Omega_{\text{VAC}} = 0.7$ in this paper.

2 DUST ATTENUATION IN GALAXIES

One of the main goals of rest-frame UV observations is to observe young and blue stellar populations which emit most of their photons in this wavelength range (e.g. Leitherer et al. 1999). From this data, we hope to estimate how many stars formed recently in a given galaxy and more generally in the Universe as a function of the redshift. However, there is a serious drawback to this: dust is quickly building up when stars evolve (Nozawa et al. 2003) and absorbed UV photons are no longer observable in UV. We have to look for them at longer wavelengths in the FIR (8–1000 μm) where dust radiates. Estimating how much of the UV flux is stolen by dust is not an obvious task. Several methods were proposed but the most popular ones are based on the slope β of the UV continuum (in the wavelength range 1200–2500 \AA), assuming a power continuum $f_\lambda \propto \lambda^\beta$, and the $F_{\text{dust}}/F_{\text{UV}}$ ratio (see Calzetti et al. 2000, for a review and papers quoted therein). The bolometric dust emission F_{dust} is computed from the $F_{\text{dust}}/F_{\text{FIR}}$ ratio and the 60 and 100 μm fluxes using the formula given in Dale et al. (2001).

A few years ago, it was suggested that UV could be self-sufficient and that UV observations by themselves could provide all the nec-

essary information to correct for dust attenuation and estimate the SFR: the slope of the UV continuum β was found to correlate with the UV dust attenuation in the central parts of starburst galaxies observed with the *International Ultraviolet Explorer* (*IUE*) (Meurer et al. 1999). However, even before *GALEX*, rest-frame UV observations showed that galaxies outside the original *IUE* sample could not quite follow this law. Moreover, the slope of the UV continuum was often estimated from the rest-frame FUV – NUV colour and another limitation comes from the flattening of the continuum at wavelengths below $\sim 1200 \text{ \AA}$ (e.g. Leitherer et al. 1999). Burgarella et al. (2005) show that the UV slope β could not be safely estimated from *GALEX* colours for galaxies at redshifts beyond about $z = 0.10\text{--}0.15$ without K corrections which, when applied without knowledge of the actual slope, introduce additional uncertainties in the measurements.

Observational evidences seem to suggest that the best way of dealing with the dust attenuation could be by involving the two wavelength ranges where these (originally) UV photons can be found (i.e. UV and FIR) to perform an energetic budget (for instance Buat & Xu 1996; Meurer et al. 1999). In parallel, sophisticated models with radiation transfer were developed (e.g. Witt & Gordon 2000; Granato et al. 2000) that showed that the UV slope β is very sensitive to the geometry and dust properties while the dispersion of the $F_{\text{dust}}/F_{\text{UV}}$ ratio is small whatever the hypothesis. In this paper, we will use the $F_{\text{dust}}/F_{\text{UV}}$ ratio to estimate dust attenuations as a reference and compare other dust estimates with it.

2.1 Two galaxy samples: a pure UV selection and a pure FIR selection

Buat et al. (2005) and Iglesias-Páramo et al. (in preparation) built two pure NUV-selected and FIR-selected samples that we will use in the rest of this paper. In brief, their samples are built from *GALEX* and *IRAS* surveys over a common 615 deg² area. Galaxies with magnitudes brighter than $\text{NUV}_{\text{AB}} = 16 \text{ mag}$ form the UV sample. The FIR sample is built from the *IRAS* PSC_z survey, which is complete down to 0.6 Jy at 60 μm . Their average distance is 53.9 Mpc for the UV-selected sample and 165.7 Mpc for the FIR-selected sample. Once objects with possible contamination are discarded, the full UV-selected sample contains 62 galaxies and the FIR-selected sample contains 118 galaxies. Note that a few objects belong to both samples. The UV data are from *GALEX* observations, the HYPERLEDA data base (Paturel et al. 2003) was used for visible observations (*UBVRI* but mostly *B* and *I*) and the FIR data from *IRAS*. All of them are corrected for galactic extinction. These two samples are representative of the local Universe: their UV and FIR luminosity functions are statistically consistent with being drawn from the same populations than the much larger samples of Wyder et al. (2005) and Takeuchi, Buat & Burgarella (2005), respectively. More details can be found in Iglesias et al. (in preparation) who deeply analysed the two galaxy samples. The median dust attenuation of the NUV-selected sample is $A_{\text{FUV}} = 1.1^{+0.5}_{-0.4}$ and that of the NUV-selected sample is $A_{\text{FUV}} = 2.9^{+1.3}_{-1.1}$ (Buat et al. 2005). In the log ($F_{\text{dust}}/F_{\text{FUV}}$) versus FUV – NUV diagram (Fig. 1), the FIR-selected sample is globally in the prolongation of the NUV-selected one. However, when we reach log ($F_{\text{dust}}/F_{\text{UV}}$) = 1.8, corresponding to $A_{\text{FUV}} = 3.5 \text{ mag}$. we see a broadening of the observed FUV – NUV colour. All these galaxies are in the FIR-selected sample. A possible interpretation of this broadening might be that the FIR emission is decoupled from the UV emission because the FIR is emitted from regions buried in dust which cannot be detected in UV. Consequently, the FUV emission would only come from a foreground layer of UV stars in

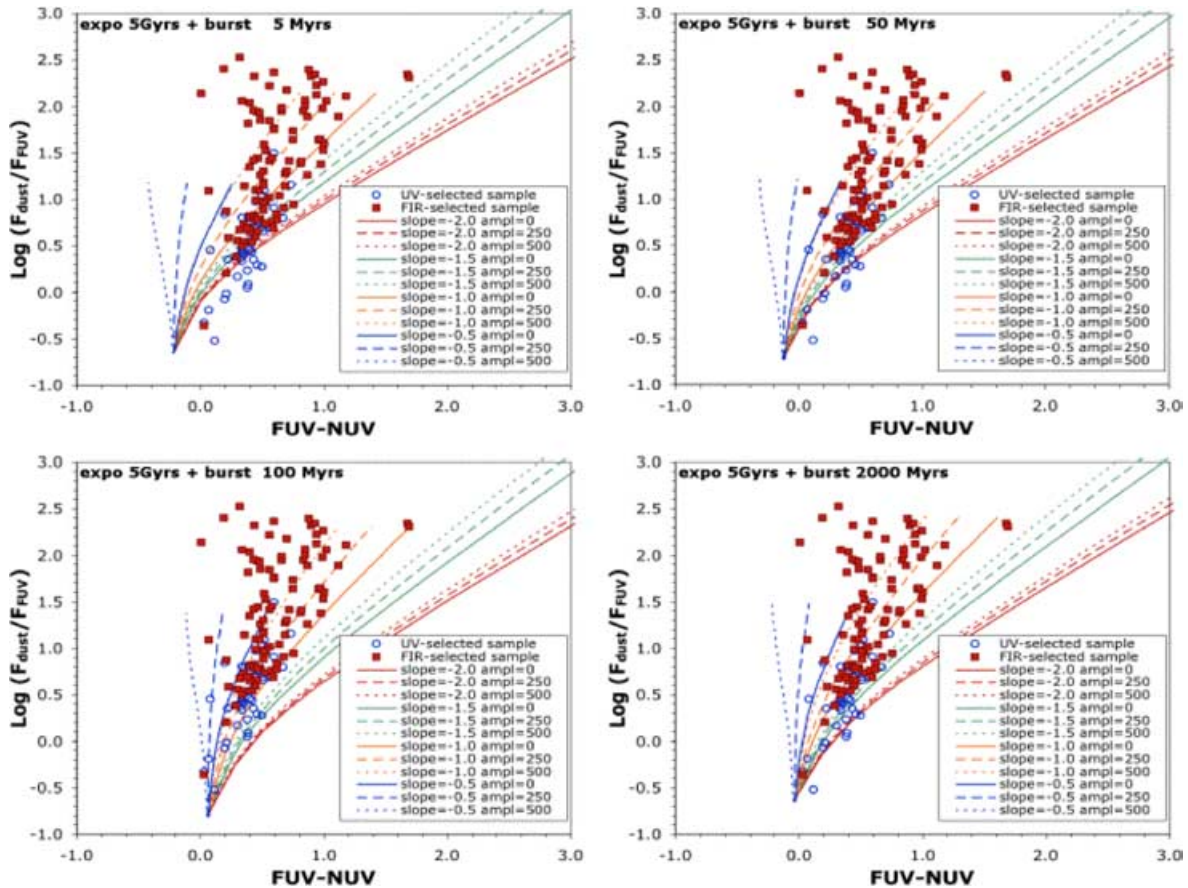


Figure 1. The UV-selected sample (open circles) and the FIR-selected sample (filled boxes) are from Buat et al. (2005). The $\log(F_{\text{dust}}/F_{\text{FUV}})$ versus FUV – NUV diagram exhibits the well-known bimodality with low dust attenuation for UV-selected galaxies and high dust attenuation for FIR-selected galaxies. The four panels from top-left to bottom-right correspond to various SFHs with an increasing age for the bursts added to an exponentially decaying 5-Gyr star formation. Several attenuation laws parametrized by the slope α and the strength of the 2175-Å bump A_{bump} are represented in each panel. The amount of dust attenuation increases along the lines (see text for more details). From right to left the first three lines correspond to a slope $\alpha = -2.0$, then -1.5 , -1.0 and -0.5 and within each group of three lines, the amplitude of the bump increases from right to left from $A_{\text{bump}} = 0$ (continuous line) to $A_{\text{bump}} = 250$ (dashed line) to $A_{\text{bump}} = 500$ (dotted line). Both the SFH and the shape of the attenuation law impact on the shape of the diagram and could explain why it is difficult to accurately estimate dust attenuation if these parameters are not accounted for.

the galaxies while the FIR would be emitted by both regions. We must be cautious, however, because those galaxies are very faint in UV with mean magnitudes in $\langle F_{\text{UV}} \rangle = 19.82 \pm 0.74$ and $\langle \text{NUV} \rangle = 18.79 \pm 0.59$, respectively. At this level, we assume that uncertainties are of the order of 0.4 and 0.3 in FUV and NUV. These uncertainties might, alternatively, be at the origin of the broadening of the sequence. The asymmetry of the distribution (only bluer colours), however, seems to suggest that this trend might be real.

2.2 The models

The main parameters driving the shape of the $\log(F_{\text{dust}}/F_{\text{FUV}})$ versus FUV – NUV (Fig. 1) is the amount of dust attenuation A_{FUV} [directly measurable from $\log(F_{\text{dust}}/F_{\text{FUV}})$; see Section 3.6] which explains the general trend observed: the more reddened the galaxies the higher the $\log(F_{\text{dust}}/F_{\text{FUV}})$ values are independently of the UV of IR selection as already described in the previous section. However, even if there is a general increasing trend of $\log(F_{\text{dust}}/F_{\text{FUV}})$ with β or FUV – NUV, quite a large dispersion is found for the present sample, as also reported by Seibert et al. (2005) and Burgarella et al. (2005) on other samples. The question, that we would like to address is whether this dispersion can be explained by one or more physical

parameters (meaning not observational errors). Kong et al. (2004) proposed that part of the dispersion is related to the effect of an additional parameter: the birthrate parameter b that is the present to past averaged SFR ratio which traces the SFH. If we use the notation of Kong et al. (2004) where the SFR is $\Psi(t)$, the birthrate parameter b is defined by

$$b = \Psi(t_{\text{present}})/\langle \Psi(t) \rangle.$$

Depending on what ‘present’ means, we can compute different values of b . The value b_0 corresponds to the instantaneous value $\Psi(t_{\text{present}})$ where present means t_0 . Other values will be introduced later on in this paper.

Kong et al. (2004) find an absolute uncertainty of 0.32 mag in A_{UV} for $b_0 > 0.3$ and about 1 mag for $b_0 < 0.3$ (corresponding respectively to high and low present star formation activity) which is still not explained. Again, is this remaining dispersion due to observational uncertainties only or are there other parameters at play?

GALEX data now covers a wide range of galaxy types and, consequently, diagrams like the $\log F_{\text{dust}}/F_{\text{FUV}}$ versus FUV – NUV one (Fig. 1) are much more populated and also more accurate than before. GALEX spectroscopy (Burgarella et al. 2005) provides us with

a hint that one of the parameters (in addition to b_0) playing a role in the general structure of the $\log(F_{\text{dust}}/F_{\text{UV}})$ versus FUV – NUV diagram might be the shape of the dust attenuation curve because they deduce from UV spectroscopy that the best S/N ratio galaxy of their sample presents a bump in the attenuation law. Note that the effect of the presence of the 2175 Å bump would be maximum in the *GALEX* NUV band at $z \approx 0$ and in the *GALEX* FUV band at $z \approx 0.4$. Building on this idea, we try to develop a simple parametric approach to model dust attenuation curves and simulate how changing it impacts this diagram. A previous parametrization of the dust attenuation laws by Charlot & Fall (2000) provided us with the original idea: they assumed an attenuation curve that follows a power law $k(\lambda) \propto \lambda^{-0.7}$. The slope of their power law is constrained by the data on starburst galaxies observed with *IUE* available before *GALEX*. They also assumed that the actual attenuation was different in regions containing young stellar populations and old stellar populations. We will adopt here a mean dust attenuation for all stellar populations without any distinction between young and old stars. However, unlike Charlot & Fall (2000) the slope of the attenuation law α can vary as can the strength of the 2175-Å bump which can be different from zero. We stress that we deal with dust attenuation laws in this paper that accounts for all possible effects undergone by all their UV photons in the presence of dust (extinction, scattering, etc.). This is different from extinction only. Here, we make the hypothesis that all our dust attenuation curves are the sum of a power law plus a Gaussian, i.e.

$$k(\lambda) = \lambda^\alpha + A_{\text{bump}} \exp^{-(\lambda - \lambda_{\text{mean}})/\sigma^2}.$$

So far, we have not changed the mean wavelength of the Gaussian (although see Fitzpatrick & Massa 1990 or Gordon et al. (2003), who found some variations in the central wavelength), fixed at 2175 Å. The width is also fixed to $\sigma = 200$ Å but we could change these two parameters if it proves that observations imply such a possibility in the future. We are left with two free parameters: the slope of the power law α with $-2.00 \leq \alpha \leq -0.25$ and the amplitude of the Gaussian A_{bump} that reproduces the UV bump in the range $0 \leq A_{\text{bump}} \leq 500$. Table 1 presents a set of parameters representative of the observed attenuation laws from Fitzpatrick & Massa (1990) and Gordon et al. (2003): Milky Way (MW); Large Magellanic Cloud (LMC); and Small Magellanic Cloud (SMC) (Calzetti et al. 1994; Charlot & Fall 2000). This table should be used as a help in the interpretation of the forthcoming analysis.

We use PEGASE 2 (Fioc & Rocca-Volmerange 1997) to compute dust-free spectra (extinction = 0 from PEGASE). To simplify the interpretation of the diagram, we limit ourselves to solar metallicity and to a Salpeter Initial Mass Function (IMF, 0.1–120 M_\odot). Moreover, no infall, no Galactic wind and no nebular emission are assumed. However, we need to assume a SFH. We select a basic exponentially decaying SFH over 10 Gyr to simulate our spectra with an e-folding time $\tau = 5$ Gyr characteristic of normal galaxies (e.g. Kennicutt 1998). In addition to this continuous SFH, one discrete burst per model in the last 5 Gyr (from 5 Myr to 5 Gyr before the end of the 10 Gyr simulated period) with a minimum duration of 100 Myr

(or less for bursts in the last 100 Myr) is added. The burst is constant over its duration. The amount of stellar mass formed in the bursts is in the range 0.5–10.0 per cent of the total mass formed during the 10 Gyr. Finally, we compute magnitudes for the 82 800 models that will be compared with the observations.

Dust moves some flux from the UV to the FIR wavelength range. It is worth noting that we compute the bolometric dust emission F_{dust} for which we do not need to know the dust temperature. Nevertheless, accounting for the dust temperature is mandatory for translating the observed fluxes at 60 and 100 μm into total dust emission. We use, here the calibration of Dale et al. (2001) based on the F_{60}/F_{100} ratio as a temperature indicator. More details are given in Buat et al. (2005) and Iglesias et al. (in preparation). The FUV and NUV dust attenuations are then simply computed by subtracting the attenuated fluxes from the unreddened ones. Fig. 1 shows how changes in the slope, the strength of the bump and the SFH could change the location of models in the $\log(F_{\text{dust}}/F_{\text{FUV}})$ versus FUV – NUV diagram and therefore the apparent calibration of the FUV – NUV colour into dust attenuation. In brief, a curve moves clockwise when the slope is steeper and/or bumps are fainter. For a given slope and bump, curves move to the lower right part of the diagram (i.e. lower $\log(F_{\text{dust}}/F_{\text{FUV}})$ and redder FUV – NUV) from young to old bursts added to the underlying exponentially decaying 5-Gyr SFH. Finally, starting for $A_{\text{FUV}} = 0$, the attenuation increases along the curve. The maximal attenuation, in Fig. 1, correspond to $A_{\text{FUV}} \approx 6$ but it increases much more quickly for shallow slopes than for steep ones. When bursts reach an age of about 100 Myr, the direction changes and models move to the top-left (higher $\log(F_{\text{dust}}/F_{\text{FUV}})$ and bluer). This change of direction in the diagram corresponds to the age when the starburst contribution decreases and the FUV – NUV colour tends to get back to the pre-burst colour, i.e. the exponentially decaying 5-Gyr SFH. We can see that a simple calibration of the FUV – NUV colour or UV slope β is not straightforward but should take into account not only the SFH as shown by Kong et al. (2004) or Granato et al. (2000) but also, very likely, the shape of the dust attenuation law (Witt & Gordon 2000). All of them impact the structure of the diagram. While the SFH and the slope change both the FUV and the NUV fluxes, the main effect of the strength of the bump is to decrease the NUV flux. Therefore, to get bump-free parameters one should therefore avoid using the rest-frame NUV band at $z \sim 0$.

2.3 The Bayesian analysis of the SEDs

The interpretation of the observed SEDs is based on a comparison of all the modelled SEDs to each observed SED. Each model is normalized to the data by minimizing χ^2 . Then the probability that a given model matches the data is quantified by a probability $\propto e^{(-\chi^2/2)}$. Models with a low probability are discarded and we keep only the best models for the determination of the galactic physical parameters. To each model are associated a set of parameters (e.g. slope of the attenuation law, age of the last burst, dust attenuation, etc.). Then, a Bayesian method is used to derive the probability that each parameter value is representative of a given galaxy. Finally, we can build a probability distribution function (PDF) for each parameter and estimate for each galaxy expectations and standard deviations from the PDF. This same method was applied by Kauffmann et al. (2003) to the SDSS data and by Salim et al. (2005) to *GALEX* + SDSS data. It must be stressed that some care must be taken when defining the input parameters (see Kauffmann et al. 2003). Indeed, the determination of the parameters could lead to incorrect results, if the input range of priors are not representative of observed values

Table 1. Parameters of the usual dust attenuation laws.

Type of attenuation	Slope	Amplitude	Mean	σ
MW	-0.90	500	2175	200
LMC	-1.00	300	2175	200
SMC	-1.20	-	-	-
Calzetti et al. (1994)	-0.95	-	-	-
Charlot & Fall (2000)	-0.70	-	-	-

and especially if it is narrower than the actual distribution because the expectations will be biased towards the most populated side of the distributions.

The originality of the present analysis lies in the constrain that the FIR data brings on the amount of dust attenuation. This is an effort to decrease the pressure on UV/optical data because there is no age-attenuation degeneracy for FIR. Another aspect that we explore is the shape of the attenuation law.

3 RESULTS

From the initial galaxy sample, some galaxies are discarded because none of our models could fit them correctly (probability below 0.50) and keep 46 UV-selected galaxies (i.e. 75 per cent of the original sample) and 103 FIR-selected galaxies (i.e. 89 per cent of the original sample). The median magnitudes/fluxes are $F_{UV} = 15.72 \pm 1.00$, $NUV = 15.35 \pm 0.99$ and $FIR = 4299 \pm 11\,476$ mJy for the UV-selected sample and $F_{UV} = 17.82 \pm 1.85$, $NUV = 17.23 \pm 1.63$ and $FIR = 4088 \pm 6426$ mJy for the FIR-selected sample. The FIR fluxes are positively skewed with a few galaxies having very large FIR fluxes, which explains that the standard deviations are larger than the median. The median dust attenuations are $A_{FUV} = 2.09 \pm 1.32$ for the sum of the two samples, $A_{FUV} = 1.39 \pm 0.65$ for the UV-selected sample and $A_{FUV} = 2.77 \pm 1.26$ for the FIR-selected samples, which is comparable to the original values quoted by Buat et al. (2005). In the following of the paper, all the quoted values are estimated from the Bayesian analysis using the FIR information unless explicitly stated otherwise, when we compare results estimated with and without FIR information.

3.1 Comparison of modelled fluxes to observed ones

Before estimating physical parameters, we must be able to reproduce correctly the observed fluxes with the models. Fig. 2 compares the modelled and observed $\log(F_{dust}/F_{FUV})$ and $FUV - NUV$. The linear correlation coefficient for the sum of the two samples (149 galaxies) is $r = 0.99$ for the modelled versus observed $\log(F_{dust}/F_{FUV})$. The linear correlation coefficient for the modelled versus observed $FUV - NUV$ is $r = 0.750$. Indeed, for this later diagram, a number of galaxies are not correctly fitted. They corresponds to the previously identified galaxies in Section 2.1 which are located in the horizontal band at very high attenuations. For these specific galaxies, the $\log(F_{dust}/F_{FUV})$ might not be a good estimator for dust attenuation if FIR and FUV are emitted in very different regions. Our models can hardly find any solutions for most of these galaxies suggesting, again, that some arbitrary part of the FIR flux might be decoupled from the UV. A possible improvement of models would be to try to add another input parameter to the fit, which would be an additional component from the FIR-only flux. If we drop galaxies lying in the top-left box at $\log(F_{dust}/F_{FUV}) > 1.80$ and $FUV - NUV < 0.60$ (13 galaxies in the FIR-selected sample, i.e. 12.6 per cent), the linear correlation coefficient reaches $r = 0.94$.

3.2 The star formation history

3.2.1 Burst age and strength in the GALEX samples

One of the issues related to UV observations is whether UV selects starbursts or not. The distribution of the age of single bursts added to the 5-Gyr exponentially decaying star formation law seems to show two denser regions: an initial one below 100 Myr and a second one at about 2 Gyr (Fig. 3). The two peaks are clearly apparent for the FIR-selected sample while it might be more likely to be

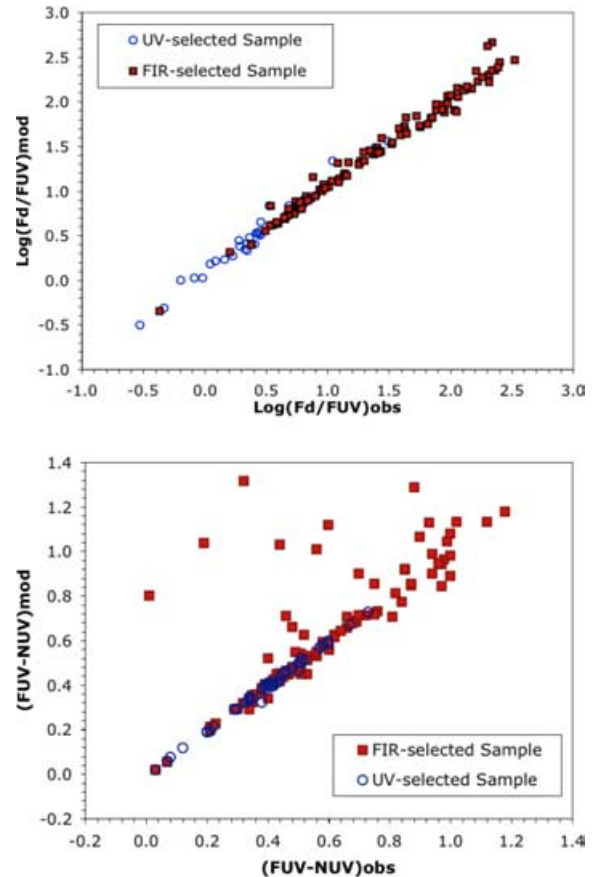


Figure 2. The two axis that form Fig. 1 are compared here: modelled versus observed $\log(F_{dust}/F_{FUV})$ and $FUV - NUV$. For the former the correlation is very good with a probability that this is not a random effect larger than 0.999. However, a few objects do not follow the general $FUV - NUV$ trend. If we take off these galaxies (discussed in the text), we have again a very significant correlation.

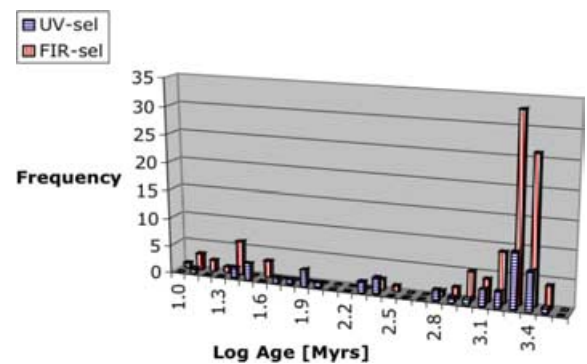


Figure 3. Histogram of the ages of the burst for our UV-selected (blue) and FIR-selected (red) samples on a large scale showing an apparent clustering at about 2 Gyr. There is also a small concentration of very young galaxies from the FIR-selected sample at ages below 50 Myr.

represented by a flatter distribution at low age for the UV-selected sample, especially if we account for the fact that our wavelength coverage is poor in between the GALEX UV range and the visible range: we lack U -band observations that would characterize bursts in the age range 0.1–1.0 Gyr (e.g. Fioc & Rocca-Volmerange 1997). A first conclusion is that about 23 per cent of the UV-selected sample

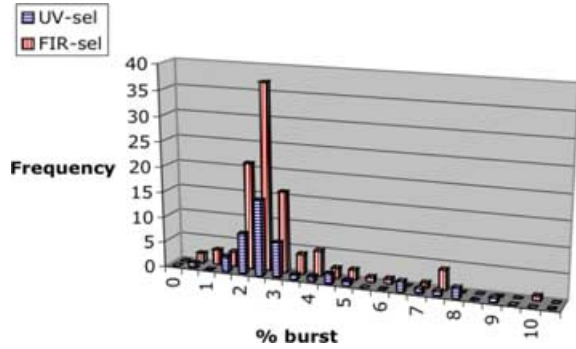


Figure 4. Histogram of the burst strength showing that most of the burst selected in the process are rather small i.e. <5 per cent. Consequently, these galaxies cannot qualify as starbursts.

and 16 per cent of the FIR-selected sample correspond to very young bursts (age <100 Myr).

The strength of the burst (represented by the percentage of the stellar mass formed in the burst) is also important to characterize the SFH. Globally, it amounts to about 2–3 per cent for our two samples (Fig. 4) which is small. For instance, Salim et al. (2005) assume the presence of bursts only when the strength would be above 5 per cent. Our SFHs are therefore consistent with continuous SFH, at least at the resolution of a few 10–100 Myr used in our work. Nevertheless, we do have a few stronger starbursts, up to 10 per cent of the stellar mass formed, for both samples: about 17 per cent for the UV-selected one and 8 per cent for the FIR-selected one.

3.2.2 The birthrate parameters

The $b = \Psi(t_{\text{present}})/\langle\Psi(t)\rangle$ parameter is widely used to measure the present-to-past SFR (e.g. Kennicutt, Tamblyn & Congdon 1994). In a recent paper, Kong et al. (2004) proposed using a value of b corresponding to the instantaneous present SFR to the averaged past SFR (see Section 2.2). However, observationally broad-band UV magnitudes (FUV and NUV for *GALEX*) are more representative of time-scales of the order of 100 Myr (e.g. Boselli et al. 2001). To account for the different time scales, we define three theoretical (i.e. directly computed by the programme from SFR ratios) values of b which differ in what ‘present’ actually means i.e. the size of the window that we call ‘present’: b_0 corresponds to Kong et al. (2004) instantaneous value, b_7 is the ratio of the SFR averaged over 10 Myr to the past SFR and b_8 is the ratio of the SFR averaged over 100 Myr to the past SFR. b_0 and b_7 are almost perfectly correlated, meaning that UV broad-band magnitudes are not very efficient in making any difference between an instantaneous and a 10-Myr burst. b_8 differs from either b_0 or b_7 (Fig. 5). b_0 and b_7 extend up to values of the order of 100: because of the shorter integration (instantaneous for b_8 and 10 Myr for b_7) the effect of a burst is major while for b_8 (integration over 100 Myr), the effect of the burst is smoothed. b_7 (and therefore b_0) can be estimated (for instance) by the $H\alpha$ line. Broad-band UV observations are averaged over a larger wavelength range and are therefore to be compared with b_8 .

3.2.3 Calibration of UV luminosities into SFR

Luminosities are known for the two galaxy samples because we know their flux and distance. The SED fitting provides us with estimates for the SFR for each galaxy through the Bayesian analysis.

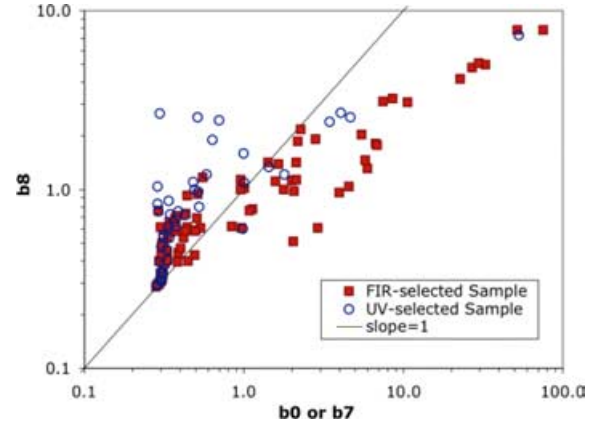


Figure 5. A comparison of the instantaneous birthrate parameter b_0 to the 100-Myr birthrate parameter b_8 shows that galaxies cluster at low b_0 while no apparent clustering is apparent for b_8 . However, the dynamics is higher for b_0 . Depending on one’s objective, the proper b value should be selected.

We are therefore able to calibrate the dust-corrected luminosities estimated from the two *GALEX* filters into SFRs. We select galaxies that have an instantaneous birthrate parameter $b_0 \leq 1.0$, meaning that the present SFR is lower than or equals the past SFR. This selection corresponds to galaxies which are not starbursting. Then, a power law is fitted to the data to give the following calibrations:

$$\text{SFR}_{\text{FUV}} = (8.895 \pm 0.250) \times 10^{-29} L_{\text{FUV}} [\text{erg s}^{-1} \text{Hz}^{-1}]$$

and

$$\text{SFR}_{\text{NUV}} = (9.225 \pm 0.260) \times 10^{-29} L_{\text{NUV}} [\text{erg s}^{-1} \text{Hz}^{-1}].$$

By construction, the above formulae are therefore applicable to non-starburst galaxies. It is interesting to note that these calibrations are almost identical to the one given by Kennicutt (1998).

3.3 The dust attenuation law

As the central wavelength and the width of the bump are defined by construction, the only free parameters of the attenuation law are the slope of the power law α and the amplitude of the bump A_{bump} . Charlot & Fall (2000) found that $\alpha = -0.7$ would be a good representation of the starburst sample presented in their paper. However, because of their sample (see Kinney et al. 1993), their dust attenuation law does not have bumps (meaning $A_{\text{bump}} = 0$ in our formalism). A MW-type dust extinction law is well represented by $A_{\text{bump}} \sim 500$ in our formalism.

Fig. 6 show the histograms of the two parameters α and A_{bump} derived for our two galaxy samples for the best analysis which used the FIR constraints.

The average (standard deviations) value of the slope is $\alpha^{\text{all}} = -1.05 \pm 0.22$ for the sum of the UV- and FIR-selected samples. This slope is marginally consistent but steeper than the value adopted by Charlot & Fall (2000) ($\alpha = -0.7$) with a tail extending to even steeper slopes, i.e. in a range similar to LMC- or SMC-like attenuation laws. The effect seems to be relatively more pronounced for the UV-selected sample ($\alpha^{\text{UV}} = -1.15 \pm 0.27$) than for the FIR-selected sample ($\alpha^{\text{FIR}} = -1.00 \pm 0.17$). The estimated uncertainties on the slopes are: $\text{err}^{\text{UV}} = 0.23$, $\text{err}^{\text{FIR}} = 0.14$ and $\text{err}^{\text{all}} = 0.17$ for the UV-selected sample.

Most of the derived A_{bump} seem to be consistent with a value $A_{\text{bump}} \sim 200\text{--}400$: $A_{\text{bump}}^{\text{all}} = 272 \pm 110$, which suggests that the 2175-Å bump is a usual feature in the attenuation curves of galaxies.

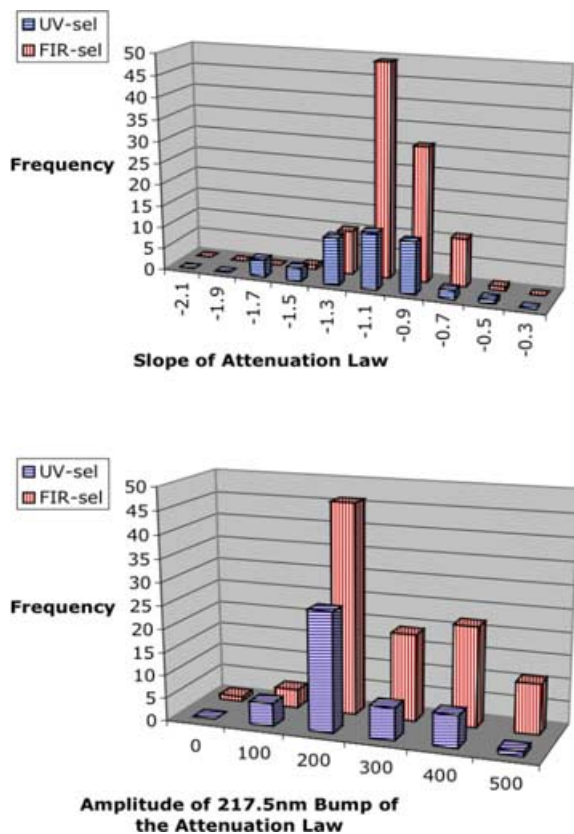


Figure 6. (a) Histogram of the slope α of the dust attenuation law for our UV-selected (blue) and FIR-selected (red) samples and (b) Histogram of the amplitude A_{bump} of the dust attenuation law for our UV-selected (blue) and FIR-selected (red) samples.

Calzetti et al. (1994) found no indication of the presence of a bump in their sample of starburst galaxies and Charlot & Fall (2000) assumed a power law without a bump. It is interesting to note that amplitudes extend to much higher values (similar to the MW one) for the FIR-selected sample $A_{\text{bump}}^{\text{FIR}} = 285 \pm 113$. The UV-selected sample mainly shows amplitudes in the ~ 200 – 300 range with $A_{\text{bump}}^{\text{UV}} = 242 \pm 97$. The uncertainties on A_{bump} is $\text{err}(A_{\text{bump}}) \sim 130$ – 140 for the UV-selected, the FIR-selected and the entire sample of galaxies. This suggests that the fitting process prefers SEDs having bumps in their attenuation laws whatever the selection.

The strength of the bump does not seem to be correlated with the slope of the attenuation law for both samples (Fig. 7). This is different to what Gordon et al. (2003) found on a sample of regions observed with *IUE* in the SMC and LMC. They suggest that the grains responsible for the 2175-Å bump would be easier to destroy than those responsible for the underlying continuum extinction. The bump strength would be anticorrelated with star formation activity evaluated by any birthrate parameter b . It is worth noting that the difference might come from the fact that we deal, here, with integrated attenuation laws and not extinction laws.

Fig. 8(a) shows that the amplitude A_{bump} of the dust attenuation bump strongly decreases from $A_{\text{bump}} = 500$ down to an amplitude of the order of 100 when the present star formation activity (b_8 is used here) increases up to $\log(b_8) = 0.0$ and then, might increase again to around $A_{\text{bump}} = 500$ but the trend is blurred by the smaller number of points at high $\log(b_8)$. As already shown in the histogram, the high amplitude part of the diagram is more populated by FIR-selected

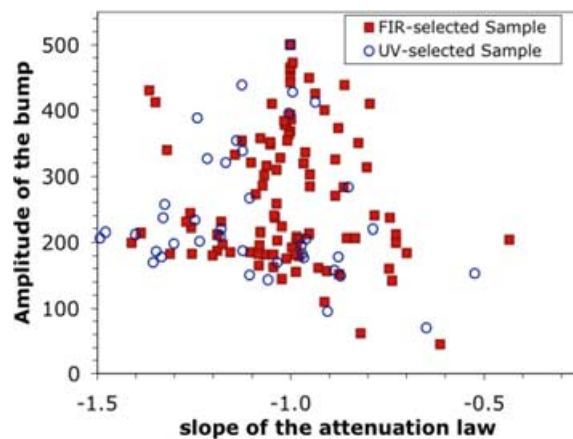


Figure 7. The amplitude of the bump and the slope of the attenuation law do not show any obvious relationship.

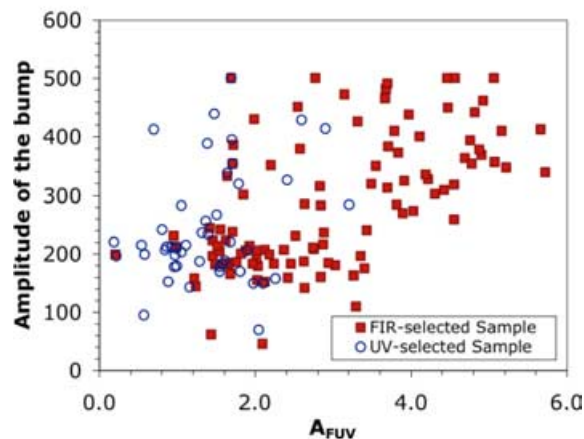
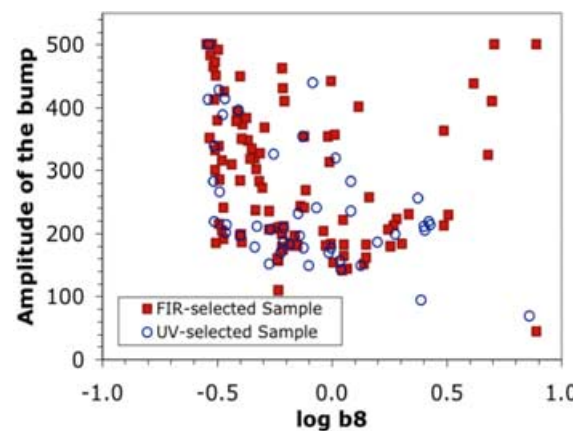


Figure 8. (a) The amplitude of the bump is decreasing with the star formation activity, evaluated with the birthrate parameter b_8 . (b) The amplitude of the bump is also correlated to the dust attenuation A_{FUV} . However, the correlation does not seem to be strong from this diagram. We can also interpret the diagram in a bimodal way with two peaks centered about $A_{\text{bump}} = 200$ and a wider one around $A_{\text{bump}} = 400$. In this case, the correlation would come from the fact that low attenuation galaxies (mainly UV-selected ones) have a fainter bump that high attenuation ones (mainly FIR-selected ones).

galaxies and the low-amplitude region by UV-selected galaxies. But both populations seem to follow the general trend. On the other hand, the slope α of the dust attenuation does not show any convincing variation and stay at about $\alpha = -1.0$. Again, we do not see any

differences between the two samples. We find something similar to what Gordon et al. (2003) found on extinction laws: the shape of the attenuation law seems to be related to the star formation activity. However, another parameter could play a role: Fig. 8(b) shows that the amplitude of the bump is correlated with the amount of dust attenuation (probability of random relation <0.1 per cent). We can see two reasons for this correlation: one would simply be because a bump is more easily detected in the presence of larger amounts of dust. A second possibility would be because the bump is more prominent (for physical reasons similar, for instance to that of Gordon et al.) in FIR-selected galaxies (or more generally highly attenuated galaxies).

In conclusion, we have found that dust attenuation laws are highly variable in terms of slopes and strength of the 2175-Å bump. The slope does not seem to be related to anything but the amplitude of the bump appears to be correlated with the star formation activity through the birthrate parameter and with the amount of UV dust attenuation A_{FUV} .

3.4 The estimation of the UV dust attenuation

Recent *GALEX* results confirmed that the amount of dust attenuation can be badly estimated from the UV slope β (e.g. Buat et al. 2005; Seibert et al. 2005; Burgarella et al. 2005). Another method for finding the amount of dust attenuation is to fit modelled SED data to observation data and to estimate dust-related parameters such as E_{B-V} , A_{FUV} and A_{NUV} . For instance, Kauffmann et al. (2003) estimated the colour excess in the z -band for the SDSS sample by fitting visible data. Salim et al. (2005) carried out the same kind of work by supplementing the SDSS data with the two *GALEX* bands. Salim et al. (2005) find an improvement of the estimation by 41 per cent on the uncertainty for A_{FUV} and A_{NUV} with respect to the estimate from SDSS data and without the UV *GALEX* fluxes. They find $\langle A_{\text{FUV}} \rangle = 1.86 \pm 0.92$ and $\langle A_{\text{NUV}} \rangle = 1.32 \pm 0.69$. Their sample is constructed by matching *GALEX* detections to SDSS spectroscopic objects. The sample is therefore close to be visibly selected and the above values should not directly compare to ours. To quantify the advantage of using the FIR flux as an additional piece of information, we perform the SED-fitting process with and without making use of the FIR information (respectively noted as +FIR and -FIR hereafter). The code predicts some FIR flux for each of the model and we are able to estimate the UV dust attenuation in the same way as if we had it from $\log(F_{\text{dust}}/F_{\text{FUV}})$.

Our results (Fig. 9 and Table 2) show quite different distributions for the UV-selected and the FIR-selected samples: the NUV-selected sample scans a range $0 < A_{\text{FUV}} < 3$ while the FIR-selected one is much broader $0 < A_{\text{FUV}} < 6$. The mean values and the average uncertainties of the estimate of individual dust attenuations in FUV and NUV for the two samples are listed in Table 2. First, the errors that we find using only UV + visible data are statistically of the same order ($\sim 0.5 - 0.6$) than those estimated by Salim et al. from their *GALEX* + SDSS analysis. However, as previously stated, we can hardly compare the absolute values of dust attenuation with previous works owing to the difference in sample definition. Assuming the same definition as Salim et al. (2005) for the improvement: $(\text{err}_{-FIR} - \text{err}_{+FIR})/\text{err}_{-FIR}$, we obtain an improvement in the error by about 70 per cent for the estimation of $\langle A_{\text{FUV}} \rangle$ and $\langle A_{\text{NUV}} \rangle$ by adding the FIR data to the UV + visible data for the UV-selected sample and by about 60 per cent for the FIR-selected sample. This is very significant and confirms that the constraint

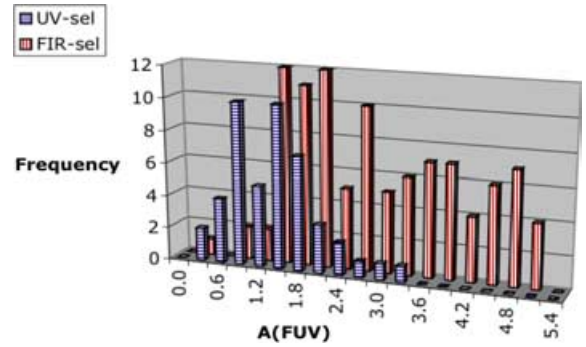


Figure 9. Histogram of the dust attenuation in FUV A_{FUV} for our UV-selected (blue) and FIR-selected (red) samples estimated from the FIR information. The two distributions are very different, as expected and consistent with previously estimated values for this sample (Buat et al. 2005; Iglesias-Páramo et al. 2005).

brought by the FIR flux is crucial for estimating dust attenuation in galaxies.

The previous results led to the conclusion that A_{FUV} and A_{NUV} cannot be correctly estimated without the FIR. Does it mean that we simply obtain a worse estimate if we do not use the FIR information? Fig. 10 suggests that it is more complex and that errors are different for both samples. On the one hand, the FIR-less processing assigns, to the UV-selected sample, overestimated UV dust attenuations by as much as 2 mag. On the other hand, it comes out with underestimated UV dust attenuations by up to 4 mag for the FIR-selected sample. The origin of this bad estimation must be found in the bad value of the FIR flux evaluated if the FIR flux is not constraining the process (Fig. 11). As expected, if we use the knowledge of the FIR flux for the sum of the two samples, the modelled-to-observed FIR flux ratio is very good: 1.15 ± 0.22 . Without the FIR, the analysis is badly constrained by the UV+visible and the ratio reaches 4.10 ± 15.47 . Interestingly enough, we observe large differences for the FIR-less analysis: the modelled-to-observed FIR flux ratio amounts to 8.84 ± 25.76 for the UV-selected sample and 1.62 ± 1.91 for the FIR-selected sample.

3.5 Dust attenuation and galaxy stellar mass

One of the products of the SED analysis is the determination of galaxy stellar masses. With our approach, dust attenuation is determined with low uncertainties and it seems interesting to revisit the mass estimates with this new information. Fig. 12(a) presents the A_{FUV} versus $\log(M/M_{\odot})$ diagram for our galaxy sample. There is a trend for UV-selected galaxies to be in the low-mass side while most FIR-selected galaxies fall in the high-mass side but we do observe, for a given mass, quite a large range of dust attenuation. For instance $10^{11} M_{\odot}$ galaxies have $1 < A_{\text{FUV}} < 5$ mag. This trend is more visible for FIR-selected galaxies but can also be observed for UV-selected ones, especially above the transition at $\log(M/M_{\odot}) \sim 10.5$ which was identified by Kauffmann et al. (2003) and can also be (less significantly) detected in our much smaller samples. In our data, low-mass galaxies do not especially relate to the UV-selected sample but the lowest mass galaxies are within the UV-selected sample and the most massive galaxies in the FIR-selected sample. Kauffmann et al. (2003) identified low-mass galaxies with young galaxies and high-mass galaxies with older ones. Fig. 12(b) shows

Table 2. Mean values for the dust attenuation in the two UV bands estimated by accounting for the FIR flux (+FIR) and without it (−FIR). The dispersions in the inferred dust attenuations [$\sigma(A_{\text{FUV}})$ and $\sigma(A_{\text{NUV}})$] correspond to the width of the distributions while the errors [$\text{err}(A_{\text{FUV}})$ and $\text{err}(A_{\text{NUV}})$] correspond to the average uncertainties on the estimates.

	UV-sel (+FIR)	FIR-sel (+FIR)	UV-sel (−FIR)	FIR-sel (−FIR)
A_{FUV}	1.41	2.95	2.02	2.58
$\sigma(A_{\text{FUV}})$	0.65	1.26	0.84	1.03
$\text{err}(A_{\text{FUV}})$	0.18	0.26	0.62	0.62
A_{NUV}	1.01	2.24	1.59	1.95
$\sigma(A_{\text{NUV}})$	0.53	1.00	0.76	0.79
$\text{err}(A_{\text{NUV}})$	0.16	0.21	0.58	0.56

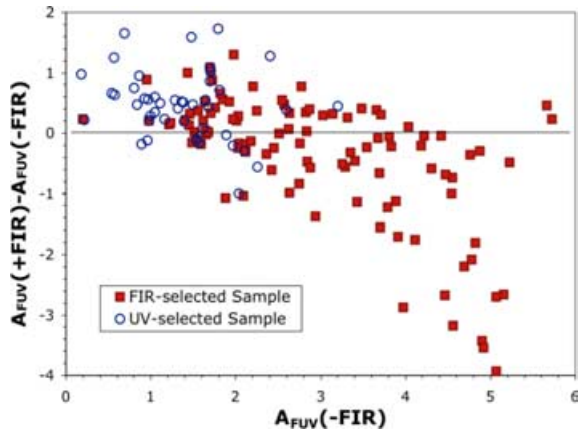


Figure 10. The FUV dust attenuation appears to be badly estimated for our UV-selected (blue) and FIR-selected (red) samples but the error is not uniformly distributed around 0. The dust attenuation seems to be overestimated for the UV-selected sample and underestimated for the FIR-selected sample.

in the b_8 versus $\log(M/M_\odot)$ diagram that we verify the same trend for our galaxies. However, we must note that the conclusion (low-mass objects are more active in star formation) might be biased. Indeed, for these kinds of galaxies, even a small change in the SFH history can produce strong changes in the resulting b_8 because the mass of stars formed in the past is small by definition. In other words, it would be more difficult for high-mass galaxies to reach high b values unless a major starburst happens. The b_0 birthrate parameter does not show any clear trend similar to the one presented in Fig. 12(b). This seems consistent with the fact that b_0 corresponds to very recent bursts which, consequently, did not have enough time to produce strong changes in the galaxy stellar mass.

3.6 Updating the $\log(F_{\text{dust}}/F_{\text{UV}})$ to A_{UV} calibrations

Buat et al. (2005) recently provided calibrations of $\log(F_{\text{dust}}/F_{\text{UV}})$ into A_{UV} for FUV and NUV based on models. Taking advantage of our two samples, we can check if such a calibration is valid for both UV- and FIR-selected samples. Fig. 13 confirms that our models do follow a law similar to Buat et al. (2005). The modelled $\log(F_{\text{dust}}/F_{\text{UV}})$ data are well correlated to the observed data with very significant correlation coefficients $r = 0.994$ in FUV and $r = 0.995$ in NUV.

Fig. 13 shows the relation between $\log(F_{\text{dust}}/F_{\text{FUV}})$ versus A_{FUV} and $\log(F_{\text{dust}}/F_{\text{NUV}})$ versus A_{NUV} , respectively. We find the follow-

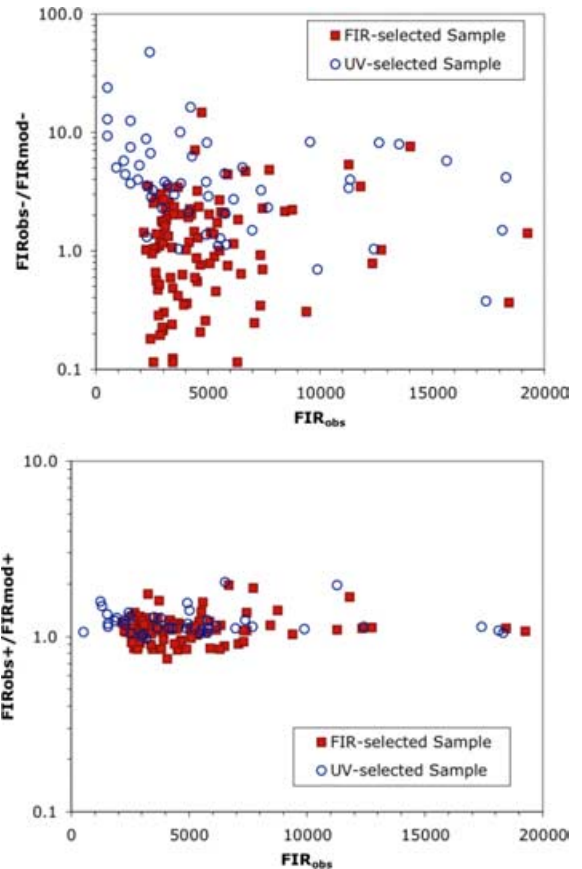


Figure 11. The origin of the bad dust attenuation estimate when we do not use the FIR data: (a) the FIR is very badly estimated (up to ± 1000 per cent) if not used as a constrain and (b) correctly (within 10–20 per cent) if we account for this important information. Note that the scales are different for the two panels.

ing laws for the two bands:

$$\begin{aligned}
 A_{\text{FUV}} &= -0.028[\log(F_{\text{dust}}/F_{\text{FUV}})]^3 \\
 &\quad + 0.392[\log(F_{\text{dust}}/F_{\text{FUV}})]^2 \\
 &\quad + 1.094[\log(F_{\text{dust}}/F_{\text{FUV}})] + 0.546, \\
 A_{\text{NUV}} &= -0.075[\log(F_{\text{dust}}/F_{\text{NUV}})]^3 \\
 &\quad + 0.639[\log(F_{\text{dust}}/F_{\text{NUV}})]^2 \\
 &\quad + 0.673[\log(F_{\text{dust}}/F_{\text{NUV}})] + 0.260.
 \end{aligned}$$

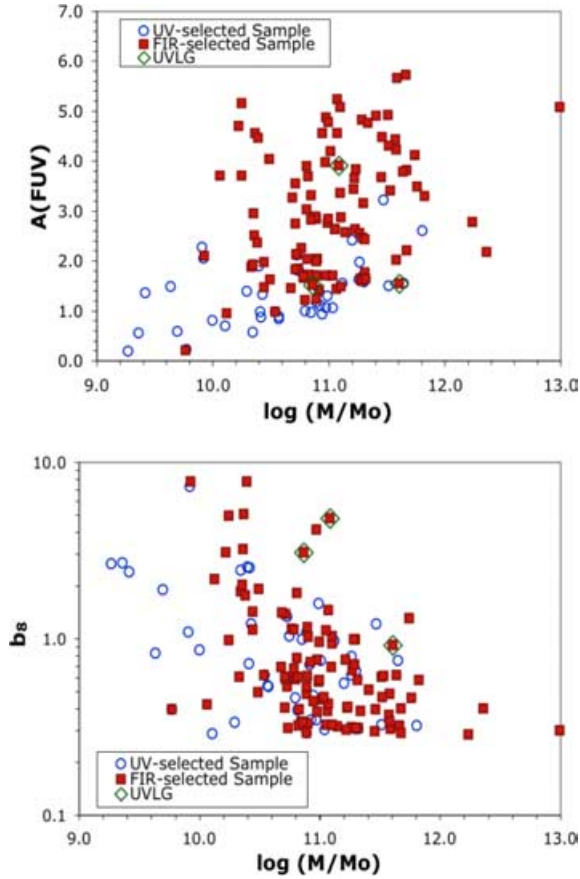


Figure 12. (a) The most massive galaxies are the most attenuated ones while the less massive ones appear to be lighter and (b) the most massive galaxies exhibit the lowest present (within 100 Myr) to past SFR: they are the oldest ones of the sample while the youngest ones are mainly UV selected and less massive. The three UVLGs detected in our sample are also plotted in these diagrams as diamonds.

Both laws are determined using the sum of the two samples. We see a continuity from the UV-selected sample (with low dust attenuations) to the FIR-selected sample (with high dust attenuations) showing that the same law could be used whatever the selection even by including various parameters such as the SFH and a very wide range of dust attenuation. The median difference between this calibration and the purely model-based calibrations in Buat et al. (2005) are small: 0.07 ± 0.19 in A_{FUV} and 0.11 ± 0.34 in A_{NUV} . This new calibration avoids obtaining negative A_{NUV} for very low $\log(F_{dust}/F_{NUV})$ values.

3.7 The origin of the structure of the $\log(F_{dust}/F_{NUV})$ versus FUV – NUV diagram

The main result of our analysis is that we can reproduce most of the structure of the $\log(A_{FUV})$ versus FUV – NUV diagram, except for a handful of galaxies with blue FUV – NUV colours and high $\log(F_{dust}/F_{NUV})$ as illustrated in Fig. 14. However, in order to understand what physical parameter(s) drive the structure of the $\log(A_{FUV})$ versus FUV – NUV diagram (which is directly related to the A_{FUV} versus FUV – NUV diagram), we have fitted a second-order polynomial to all our galaxies (i.e. 151 galaxies from the UV-selected + FIR-selected samples). The best-fitting law with a

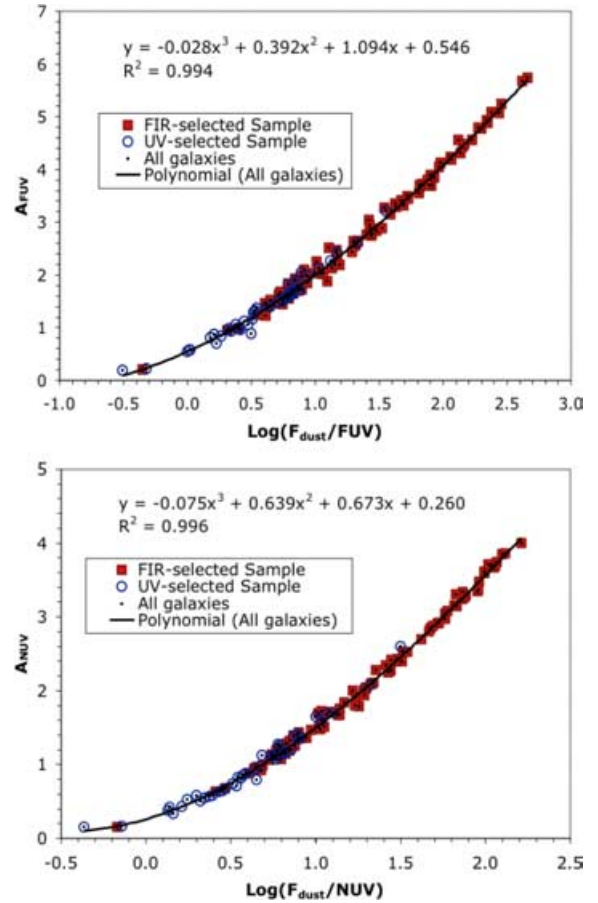


Figure 13. (a) The observed and modelled A_{FUV} versus $\log(F_{dust}/F_{FUV})$ for our UV-selected (blue) and FIR-selected (red) samples and (b) the calibration of $\log(F_{dust}/F_{NUV})$ for our UV-selected (blue) and FIR-selected (red) samples into A_{NUV} .

correlation coefficient $r = 0.837$ is significantly different from a random one at a level >0.999 .

Then, we subtract the contribution from this parameter (through the modelled relation) and we try to explain, after each step, the remaining dispersion by correlating it with new parameters (namely the amplitude of the bump A_{bump} , the slope of the attenuation law α and the birthrate parameters b_0 and b_8). To estimate the validity of each of the tested parameters, we have two quantitative tools: the correlation coefficient (corresponding to the quality of the fitted law i.e. first- or second-order polynomials) and the variation of the remaining dispersion evaluated by the mean and standard deviation which should be very close to zero for the mean and decreasing for the standard deviation. Table 3 summarizes the results for each iteration. We assume that a parameter adds some useful information if the probability that the distribution is different from a random one, evaluated from the correlation coefficient and the number of degrees of freedom, is below 0.05.

We can see that, for the whole sample, the residual dispersion after removing the FUV – NUV trend is $\sigma(\text{residual}) = 0.722$ of which 53.8 per cent can be explained as follows: 9.4 per cent by the influence of the bump; 34.2 per cent (the main contribution) from the influence of the slope of the attenuation law (α); and 10.2 per cent by the influence of $\log(b_0)$. The top three parameters in decreasing order are therefore α , A_{bump} and $\log(b_0)$. The remaining $\sigma(\text{residual}) = 0.333$ i.e. 46.2 per cent of the initial one cannot be explained with a

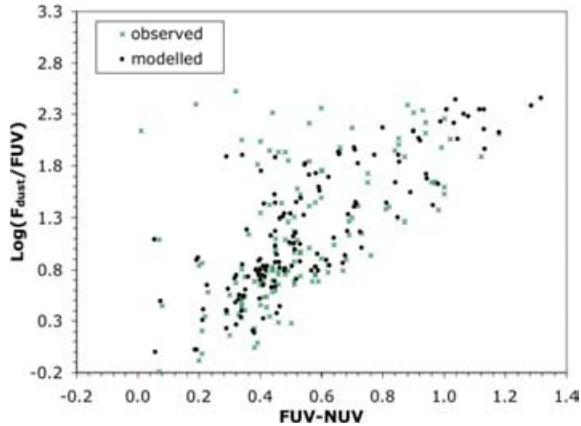


Figure 14. The comparison of the observed (crosses) and modelled (dots) diagram is rather good for all parts of the diagram, suggesting that our physical parameters are enough for the process to find a good solution both in UV and in FIR. However, the program fails to find solution for galaxies which are, at the same time rather blue (i.e. $FUV - NUV < 0.5$ and with extreme attenuations ($A_{FUV} > 2.0$).

sufficient significance by any combination of parameters. Observational uncertainties are of this order and they are likely to be the final contribution but we cannot rule out any additional parameters such as a purely FIR contribution as suggested before. Replacing $\log(b_0)$ by $\log(b_8)$ gives less information because the remaining residual is 0.388 i.e. only 46.3 per cent of the dispersion is explained by the combination of the three parameters: α , A_{bump} and $\log(b_8)$. Unfortunately, none of these parameters can be inferred from broad-band observables. We tried several colours and luminosities but no one can give a satisfactory explanation. The best one seems to be a colour involving the NUV (because of the influence of both the bump and the slope) and a red magnitude (because of the information on the present-to-past SFR). For instance the NUV-I colour can only explain less than 10 per cent of the dispersion for the whole galaxy sample and it seems very difficult to give any recipe that could be

used to estimate the UV dust attenuation from broad-band observables valid for any sample.

3.8 A backup recipe when no FIR data is available for UV-selected galaxies

Although physically very informative for understanding the structure of the $\log(F_{\text{dust}}/F_{\text{FUV}})$ versus FUV – NUV diagram, the previous section lead us to a rather negative conclusion. However, we used a severe approach because we wished to find a recipe for the sum of both the UV-selected and the FIR-selected sample. One might correctly argue that trying to find an exit to the FIR-selected sample is not useful because of the availability of the FIR data. It is therefore possible to compute $\log(F_{\text{dust}}/F_{\text{FUV}})$ and therefore estimate the UV dust attenuation with low uncertainties for these galaxies. However, this is often impossible for UV-selected galaxies, especially as soon as we are looking to the high-redshift Universe. Consequently, we will try to find the best solution to estimate dust attenuation for UV-selected galaxies when F_{dust} is not available. Table 4 summarizes the results for each iteration as in the previous section for the UV-selected sample.

The first point is that residuals are globally smaller ($\sigma(\text{residual}) = 0.433$) for the UV-selected sample than for the UV-selected plus FIR-selected samples. It might mean that less parameters are acting or might be due to brighter magnitudes and we cannot make any conclusions. However, we can proceed in a relative way. The strength of the bump A_{bump} presents a lower influence with a low coefficient correlation and even a slight increase of the dispersion as compared to the post-FUV – NUV residuals. The correlation coefficient is low and we will assume that the effect of this parameter is below our detectability threshold as compared to the uncertainties. This conclusion must be associated with the previous correlation of the bump strength with the amount of dust attenuation: UV-selected galaxies present less prominent bumps. The role of the slope α of the dust attenuation law is still major because it explains 22.4 per cent of the dispersion. The birthrate parameter $\log(b_0)$ explains an additional 10.6 per cent while $\log(b_8)$ does not bring anything statistically.

Table 3. Evolution of the residuals for the whole UV-selected plus FIR-selected samples after subtraction of the influence of each significant parameter for 151 galaxies. The parameter (noted x) listed in the first column should be used in the second column. Note that the probability that the relation are due to a pure random association are always below 0.01.

Parameter (x)	A_{FUV}	Correlation coefficient	Mean of residuals	$\sigma(\text{residual})$
FUV – NUV	$-0.6721x^2 + 4.4884x + 0.1958$	0.8372	-0.003	0.722
A_{bump}	$0.0028x - 0.7587$	0.4237	-0.001	0.654
Slope α	$1.8928x^2 + 6.3803x + 4.5132$	0.7828	0.000	0.407
$\log(b_0)$	$0.4125x + 0.0554$	0.5738	0.000	0.333
$\log(b_8)$	$0.5090x + 0.0696$	0.4281	-0.001	0.388
NUV-I	$0.1597x^2 + 1.1943x + 2.0138$	0.4069	-0.002	0.659

Table 4. Evolution of the residuals for the UV-selected sample only, after subtraction of the influence of each significant parameter for 46 galaxies.

Parameter (x)	A_{FUV}	Correlation coefficient	Mean of residuals	$\sigma(\text{residual})$
FUV – NUV	$1.4168x^2 + 2.1207x + 0.3477$	0.7470	0.000	0.433
A_{bump}	$0.0008x - 0.1990$	0.2762	0.005	0.441
Slope α	$0.9956x + 1.1494$	0.6315	0.000	0.336
$\log(b_0)$	$0.3905x + 0.1058$	0.5055	0.000	0.290
$\log(b_8)$	$0.5090x + 0.0696$	0.1241	0.000	0.333
NUV-I	$0.3298x^2 + 2.7465x + 5.4931$	0.6669	-0.001	0.323

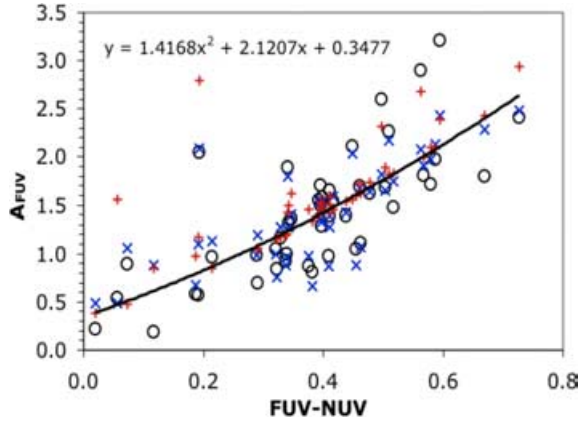


Figure 15. Comparison of the original A_{FUV} versus FUV – NUV diagram to the model-based and the observable-based re-constructed diagrams. The physical reconstruction from model-based parameters (crosses) follows very satisfactorily the observed points (circles). Although the quality of the reproduction is worse if the recipe using the FUV – NUV and NUV – I colour is used (pluses), especially at FUV – NUV > 0.5, it is better than the second-order polynomial only.

The combination of α and $\log(b_0)$ amounts to 33.0 per cent, that is much less than for the whole sample. However, the absolute value of the residuals is much smaller (0.190 versus 0.333) and it might be difficult to reach absolute uncertainties lower than 0.19. However, the median FUV magnitude for the whole sample is $\text{FUV} = 16.7 \pm 1.9$ while it is $\text{FUV} = 15.7 \pm 1.0$ for the UV-selected sample and we expect uncertainties to be smaller for the latter which, in turn, might explain the absolute low residuals, but again we cannot rule out another unknown parameter. *GALEX* FUV – NUV and NUV – I colours could be used to estimate A_{FUV} for UV-selected galaxies:

$$A_{\text{FUV}} = 1.4168(\text{FUV} - \text{NUV})^2 + 0.3298(\text{NUV} - I)^2 + 2.1207(\text{FUV} - \text{NUV}) + 2.7465(\text{NUV} - I) + 5.8408.$$

Fig. 15 shows how the physical parameter-based and the observable-based points in the $\log(F_{\text{dust}}/F_{\text{FUV}})$ versus FUV – NUV diagram compare with the original observed ones. We must stress that the relation inferred from the two colours for estimating the UV dust attenuation has a final uncertainty of the order 0.323 for our sample, independently of the value of any physical parameters. This seems reliable because Kong et al. (2004) found an uncertainty of 0.32 mag for galaxies with $b_0 > 0.3$ but approximately 1 mag for lower b_0 . Here only six galaxies (i.e. 13 per cent) have $b_0 < 0.3$ but 40 per cent have $b_0 \leq 0.31$.

3.9 Ultraviolet luminous galaxies

Heckman et al. (2005) found in the first matched set of *GALEX* and SDSS data 74 nearby ($z < 0.3$) galaxies with FUV luminosities larger than $2 \times 10^{10} L_{\odot}$ and called them UV luminous galaxies (UVLGs). Heckman et al. (2005) noted that these objects have similarities with LBGs: FUV dust attenuations of 0.5–2 mag, SFRs of 3–30 $M_{\odot} \text{yr}^{-1}$. Two classes of UVLGs are suggested: (1) massive and large ones with $M \sim 10^{11} M_{\odot}$, intermediate optical–UV colours, birthrate parameters of the order of (1) and metal-rich and (2) low-mass and compact ones with $M \sim 10^{10} M_{\odot}$, blue optical–UV colours, starburst-like birthrate parameters and subsolar metallicities.

Applying the same criterium to the luminosity, we find three galaxies in our samples belonging to the UVLG class. Two of them

are FIR selected and the last one belongs to both the UV- and the FIR-selected samples. Their mean luminosity is $\langle L_{\text{UVLG}} \rangle = 3.0 \times 10^{10} \pm 0.93 \times 10^{10} L_{\odot}$. Their mean birthrates are $\langle b_0 \rangle = 11.6 \pm 13.7$ and $\langle b_g \rangle = 2.9 \pm 1.9$ meaning that these objects are active star-forming galaxies. Indeed, their mean SFR are high ($\text{SFR} = 39.4 \pm 18.0 M_{\odot} \text{yr}^{-1}$). Their FUV dust attenuation estimated from $\log(F_{\text{dust}}/F_{\text{FUV}})$ is $\langle A_{\text{FUV}} \rangle = 2.32 \pm 1.38$ mag, slightly above the upper limit given by Heckman et al. (2005). One of them almost reaches $A_{\text{FUV}} = 4$ mag (Fig. 12). We do find that the attenuations of Heckman et al. (2005) for the three UVLGs in the sample of Buat et al. (2005) sample are underestimated as was found for FIR-selected galaxies in Section 3.4. Their masses are above the transition at $\sim 3 \times 10^{10} M_{\odot}$ (Fig. 12), they resemble the large UVLGs defined by Heckman et al. (2005).

We also looked for UVLGs in the sample of galaxies from Goldader et al. (2002). These galaxies are also plotted in Fig. 16. One of them: VV114 has a UV luminosity corresponding to UVLGs: VV114 FIR luminosity is $\log(L_{\text{FIR}}) = 11.7$ i.e. a luminous infrared galaxy (LIRG). The spectroscopic sample of Burgarella et al. (2005) contains one UVLG with a rest-frame luminosity (its redshift is $z = 0.286$) of $\sim 2 \times 10^{10} L_{\odot}$. This galaxy presents a FIR luminosity of $\log(L_{\text{FIR}}) = 11.0$ and is also a LIRG. The log SFR amounts to 1.41, in the upper part of the range for large UVLGs of Heckman et al. (2005). The colours published by Burgarella et al. (2005) are observed colours and, from the spectroscopic slope β of the UV continuum, we estimated K-corrected FUV – NUV. In Fig. 16, these LIRGs are on the left part of the diagram and their observed/modelled location are very close to the observed UVLGs. We also plot the LBG cB58 (Baker et al. 2002), which is located below the bulk of galaxies in our sample, i.e. in a different place from the above galaxies. It seems therefore that massive UVLGs might be associated to LIRGs. To check whether the location in the $\log(F_{\text{dust}}/F_{\text{FUV}})$ versus FUV – NUV diagram is consistent with the location of ULIRGs, we overplot in Fig. 16 all the LIRGs from Burgarella et al. (2005). Both the UVLGs of our sample and those LIRGs approximately share the same zone of the diagram, perhaps indicating some link between them.

4 CONCLUSION

We compared multiwavelength data of a FIR-selected sample and a UV-selected sample to a set of 82 800 models. We built the models

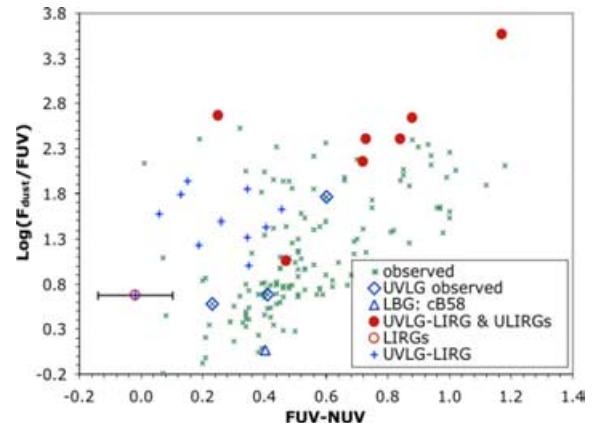


Figure 16. The location of UV luminous galaxies in our sample corresponds to the location of LURGs in the $\log(F_{\text{dust}}/F_{\text{FUV}})$ versus FUV – NUV diagram drawn from the spectroscopic sample of Burgarella et al. (2005) represented as pluses and Goldader et al. (2002) represented as filled dots.

in two phases: (i) we use PEGASE 2 to form dust-free spectra (solar metallicity, Salpeter 0.1–120 M_{\odot} IMF and several SFHs (5-Gyr decaying exponential plus one burst with age in the range 5–5000 Myr) and (ii) we estimate the amount of dust attenuation assuming different attenuation laws formed by a power law with a slope α plus a Gaussian which reproduces approximately the 2175-Å bump. For the Gaussian, only the strength of the bump can change while the position of the bump and its width are kept constant for a sake of simplicity and in relatively good agreement with what is observed.

The comparison between observations and models is carried out via a Bayesian approach which allows to statistically estimate the best value for each parameter and the associated uncertainties probabilistically.

The first important result is that it is not possible to accurately estimate the UV dust attenuation without information on the FIR flux. The errors can be as large as +2 mag (overestimated in average by 0.5 ± 0.6 in A_{FUV}) for the UV-selected sample and –4 mag (underestimated in average by 0.4 ± 1.0 in A_{FUV}) for the FIR-selected sample.

Globally, our models reproduce rather well the observed data except for a few objects which appears to present very extreme dust attenuations similar to ULIRGs. For these objects, it might be that the FIR flux is decoupled from the UV flux, which might mean that the $\log(F_{dust}/F_{FUV})$ has difficulty in providing us with good estimates for the dust attenuations. However, even in the FIR-selected sample, only about 10 per cent of the galaxies are like this.

In the remainder of the work, we use the FIR information to estimate the galaxy physical parameters, which allows us to decrease the pressure on the UV/optical range by constraining the absolute amount of attenuation with the FIR flux. We confirm that the UV dust attenuation is much lower on average (~ 1.4 mag) for UV-selected galaxies than for FIR-selected galaxies (~ 3.0 mag). We find that small bursts (mainly below 5 per cent) need to be added to the underlying continuous SFH to reproduce the data. The age of these bursts can be very young (< 100 Myr) or rather old (~ 2 Gyr), but with the present data, the intermediate range seems to be poorly populated (but more U -band data are required to confirm this trend).

The shape of attenuation laws strongly departs from bump-free laws. Both the slope α and the strength of the bump change, which mean that the correction applied to the UV flux (at low or high redshift) are generally wrong if a bump is not accounted for: in average, an attenuation law with the characteristics of the LMC attenuation law seems to be more representative of the average galaxy in the UV-selected sample and an even stronger bump for IR-selected galaxies. We recalibrated the dust attenuations from the $\log(F_{dust}/F_{FUV})$ and $\log(F_{dust}/F_{NUV})$ in the *GALEX* FUV (A_{FUV}) and NUV (A_{NUV}), respectively.

The $\log(F_{dust}/F_{FUV})$ versus FUV – NUV diagram presents some dispersion about an average law which is explained (by order of decreasing relevance) by the variation of the slope of the attenuation law and the instantaneous birthrate parameter b_0 for the UV-selected sample. For the FIR-selected sample, the strength of the bump also gives some explanation. From our analysis, we find that none of these parameters can be estimated correctly from broad-band photometry. However, spectroscopy might help.

Finally, we develop a recipe that allows us to estimate the FUV dust attenuation A_{FUV} from the FUV – NUV and the NUV – I colours for UV-selected galaxies. However, this recipe is less accurate than the $\log(F_{dust}/F_{FUV})$ method and should only be used when no FIR data is available.

ACKNOWLEDGMENTS

We are grateful to S. Charlot who frequently discussed the topic of this article with us, T. Heckman and D. Calzetti who helped us during a summer stay in Baltimore. We also thank the French Programme National Galaxies and Programme National de Cosmologie for financial support.

REFERENCES

- Baker A. J., Lutz D., Genzel R., Tacconi L. J., Lehnert M. D., 2002, *A&A*, 372, L37
- Barmby P. et al., 2004, *ApJS*, 154, 97
- Bell E. F., 2002, *ApJ*, 577, 150
- Boselli A., Gavazzi G., Donas J., Scodreggio M., 2001, *AJ*, 121, 753
- Bouwens R. J. et al., 2004, *ApJ*, 616, 79
- Buat V., Xu C., 1996, *A&A*, 306, 61
- Buat V. et al., 2005, *ApJ*, 619, L51
- Bunker A. J., Stanway E. R., Ellis R. S., McMahon R. G., 2004, *MNRAS*, 355, 374
- Burgarella D. et al., 2005, *ApJ*, 619, L63
- Calzetti D., Kinney A. L., Storch-Bergmann T., 1994, *ApJ*, 429, 582
- Calzetti D., Armus L., Bohlin R. C., Kinney A. L., Koorneef J., Storch-Bergmann T., 2000, *ApJ*, 533, 682
- Charlot S., Fall S. M., 2000, *ApJ*, 539, 718
- Dale D. A., Helou G., Contursi A., Silbermann N. A., Kolhatkar S., 2001, *ApJ*, 549, 215
- Efstathiou A., Rowan-Robinson M., 2003, *MNRAS*, 343, 322
- Fioc M., Rocca-Vomerange B., 1997, *A&A*, 344, 399
- Fitzpatrick E. L., Massa D., 1990, *ApJS*, 72, 163
- Flores H. et al., 1999, *ApJ*, 517, 148
- Forster Schreiber N. M. et al., 2004, *ApJ*, 616, 40
- Goldader J. D., Meurer G., Heckman T. M., Seibert M., Sanders D. B., Calzetti D., Steidel C. C., 2002, *ApJ*, 568, 651
- Gordon K. D., Clayton G. C., Misselt K. A., Landolt, Arlo U., Wolff M. J., 2003, *ApJ*, 594, 279
- Granato G. L., Lacey C. G., Silva L., Bressan A., Baugh C. M., Cole S., Frenk C. S., 2000, *ApJ*, 542, 710
- Heckman T. M. et al., 2005, *ApJ*, 619, L35
- Kauffmann G. et al., 2003a, *MNRAS*, 341, 33
- Kauffmann G. et al., 2003b, *MNRAS*, 341, 54
- Kennicutt R. C., 1998, *ARA&A*, 36, 189
- Kennicutt R. C., Tamblyn P., Congdon C. E., 1994, *ApJ*, 435, 22
- Kinney A. L., Bohlin R. C., Calzetti D., Panagia N., Wyse R. F. G., 1993, *ApJS*, 86, 5
- Kong X., Charlot S., Brinchmann J., Fall S. M., 2004, *MNRAS*, 349, 769
- Leitherer C. et al., 1999, *ApJS*, 123, 3
- Martin D. C. et al., 2004, *ApJ*, 619, L1
- Meurer G. R., Heckman T. M., Calzetti D., 1999, *ApJ*, 521, 64
- Motta V. et al., 2002, *ApJ*, 574, 719
- Nozawa T., Kozasa T., Umeda H., Maeda K., Nomoto K., 2003, *ApJ*, 598, 785
- Paturel G., Petit C., Prugniel Ph., Theureau G., Rousseau J., Brouty M., Dubois P., Cambresy L., 2003, *A&A*, 412, 45
- Salim S. et al., 2005, *ApJ*, 619, L39
- Seibert M. et al., 2005, *ApJ*, 619, L55
- Shapley A. E., Steidel C. C., Adelberger K. L., Dickinson M., Giavalisco M., Pettini M., 2001, *ApJ*, 562, 95
- Steidel C. C., Giavalisco M., Pettini M., Dickinson M., Adelberger K. L., 1996, *ApJ*, 462, L17
- Takeuchi T. T., Buat V., Burgarella D. 2005, *A&A*, submitted
- Williams R. E. et al., 1996, *AJ*, 112, 1335
- Witt A. N., Gordon K. D., 2000, *ApJ*, 528, 799
- Wyder T. K. et al., 2005, *ApJ*, 619, L15
- Yan H. et al., 2004, *ApJ*, 616, 63

This paper has been typeset from a $\text{\TeX}/\text{\LaTeX}$ file prepared by the author.